Numerical calculations of plasma response to external magnetic perturbations in tokamaks

Juhyung Kim[1], S. S. Kim[1] and Hogun Jhang[1]

[1]National Fusion Research Institute, Rep. Korea

Corresponding Author: yegakjh@nfri.re.kr

Abstract:

Numerical studies are made of the effects of resistivity on linear plasma responses to resonant magnetic perturbations (RMPs) in tokamaks based on a reduced magnetohydrodynamic (MHD) model. From a local two-field model, it is suggested that the ratio of the poloidal electron advection to the resistivity diffusion rate $\alpha_{\rm m}$ can be a figure of merit parameter in linear RMP penetration physics. Global simulations using a four-field model show that there exists an effective threshold of the perpendicular electron flow ($V^c_{e,\perp}$) beyond which RMPs cannot penetrate. At low resistivity, small $V^c_{e,\perp}$ renders the RMP penetration sensitive to the change in q_{95}. The kink response is observed to be closely related to the residual level of RMPs at rational surfaces and can be also strongly affected by resistivity. In addition, the preliminary result on the RMP effects on ELM simulations is presented.

1 Introduction

Controlling edge-localized-modes (ELMs)[1–3] in tokamak H-mode operation has been a major focus in the magnetic fusion community for the past decades. One of popular approaches for controlling ELMs is the application of resonant magnetic perturbations (RMPs)[2, 3] into the plasma. Current understanding of the ELM control by RMPs is that the externally applied RMP penetrates into the plasma, modifies magnetic topology, otherwise well nested, and destroys good flux surfaces by generating the regions of stochastic magnetic fields. The stochastic magnetic fields, in turn, enhance plasma transport and reduce steep gradients in edge pedestal parameters, resulting in the mitigation or even the suppression of ELMs.

We consider collisional effects on linear plasma responses in the RMP penetration. Experimentally, it has been known that in low collisionality plasmas, effective mitigation (or suppression) is sensitive to RMP specifications, such as current configuration of RMP coils.[4, 5] In contrast, the details of RMP configuration are not a decisive factor at high collisionality.[2, 6]

Previous works[7–9] have identified that resistivity diffuses current perturbations induced by plasma rotation at rational surfaces, reducing $\delta B_r^{\rm plas}$. RMPs can easily affect magnetic topology at high resistivity, while they cannot penetrate into the plasma at low resistivity, due to the development of a strong screening current. Only when electron perpendicular flow[10, 11] is nearly zero, $V_{e,\perp} \simeq 0$, RMPs can penetrate into the plasma and produce this stochastic field

regions at low resistivity. Theses are observed in the two-fluid magnetohydrodynamic (MHD) modeling.[8, 12] This zero flow condition may be relaxed in more resistive plasmas. However, there remains a question of how large deviation of $V_{e,\perp}$ from the zero flow condition is allowed for RMP penetration at given resistivity.

In this work, we study collisional effects on plasma responses to RMPs and its implication on the basis of a four-field reduced MHD model[13], using the BOUT++ framework[14].

2 Plasma Response Model

The plasma response in this study is modeled by a set of reduced MHD (RMHD) [13] equations consisting of the time evolution of vorticity, parallel ion flow, pressure and the Ohm's law,

$$\frac{1}{v_A^2}\frac{\mathrm{d}U}{\mathrm{d}t} = \frac{B_0^2}{\bar{B}^2}\nabla_\parallel J_{\parallel \mathrm{t}} + \hat{\boldsymbol{b}}_0 \cdot \boldsymbol{\kappa}_0 \times \boldsymbol{\nabla}_\perp p_1 \,, \tag{1a}$$

$$\frac{\partial \psi^{\mathrm{plas}}}{\partial t} + \frac{1}{B_0}\nabla_\parallel B_0 \phi = \eta J_{\parallel 1} + \boldsymbol{\nabla}\psi^{\mathrm{tot}} \times \hat{\boldsymbol{b}}_0 \cdot V_{e,\perp}\hat{\boldsymbol{r}} \,, \tag{1b}$$

$$\frac{\mathrm{d}V_\parallel}{\mathrm{d}t} = -\frac{1}{2}v_A^2\left(\nabla_\parallel p_1 - \hat{\boldsymbol{b}}_0 \cdot \boldsymbol{\nabla} p_0 \times \boldsymbol{\nabla}\psi^{\mathrm{tot}}\right) \,, \quad \text{and} \tag{1c}$$

$$\frac{\mathrm{d}p_1}{\mathrm{d}t} + \hat{\boldsymbol{b}}_0 \cdot \boldsymbol{\nabla}_\perp \phi \times \boldsymbol{\nabla} p_0 = \hat{\beta}\left(2\hat{\boldsymbol{b}}_0 \cdot \boldsymbol{\nabla}\phi \times \boldsymbol{\kappa}_0 - \nabla_\parallel V_\parallel\right) \,, \tag{1d}$$

where $U = \nabla_\perp^2 \phi$ is vorticity, $J_{\parallel \mathrm{t}} = J_{\parallel 0} - J_{\parallel 1}$ is the normalized total parallel current density with an equilibrium parallel current $J_{\parallel 0}$ and a fluctuating current $-J_{\parallel 1} = -\nabla_\perp^2 \psi^{\mathrm{plas}}$, $\psi^{\mathrm{tot}} = \psi^{\mathrm{plas}} + \psi^{\mathrm{vac}}$ is the magnetic fluctuation with a vacuum field, $\delta\boldsymbol{B}^{\mathrm{vac}} = \boldsymbol{\nabla}\psi^{\mathrm{vac}} \times \boldsymbol{B}_0$ and a plasma driven field, $\delta\boldsymbol{B}^{\mathrm{plas}} = \boldsymbol{\nabla}\psi^{\mathrm{plas}} \times \boldsymbol{B}_0$, and p_0 and p_1 are normalized equilibrium and perturbed pressure, respectively. Electrostatic and magnetic vector potentials are given by $\Phi = B_0\phi$ and $\boldsymbol{A} = \boldsymbol{A}_0 - \boldsymbol{B}_0\psi$, respectively. In addition, the nominal Alfvén velocity $v_A^2 = \bar{B}/(\mu_0\rho)^{1/2}$, the sound speed $v_s = (5P_0/3\rho)^{1/2}$, and $\hat{\beta} \equiv 2v_S^2/(v_A^2 + \bar{B}^2 v_S^2/B_0^2)$ are defined in terms of the maximum magnetic field, $\bar{B} = \max(B_0)$. The total time derivative and the parallel derivative are $\mathrm{d}f/\mathrm{d}t = \partial f/\partial t + [\phi, f]$ and $\nabla_\parallel f \equiv \hat{\boldsymbol{b}}_0 \cdot \boldsymbol{\nabla} f - [\psi^{\mathrm{tot}}, f]$, respectively, where $[f, g]$ is the conventional Poisson bracket operation, $[f, g] = \hat{\boldsymbol{b}}_0 \cdot \boldsymbol{\nabla} f \times \boldsymbol{\nabla} g/B_0$.

In Ohm's law, Eq. (1)(b), the perpendicular electron drift, $V_{e,\perp}$, consists of the $\boldsymbol{E} \times \boldsymbol{B}$ and the diamagnetic drift velocity, $V_{e,\perp} = E_{r0}/B_0 + (v_A^2/2\Omega_i)\mathrm{d}p_{e0}/\mathrm{d}r$, where $\Omega_i = eB_0/m_i$. E_{r0} is an equilibrium radial electric field and p_{e0} is the normalized electron pressure. Electron pressure fluctuations are neglected. Hereafter, the electron perpendicular drift is simply referred to as "rotation".

The RMHD model, Eq. (1), with vacuum perturbations is implemented in the BOUT++ framework[14] in a tokamak geometry. The simulation size is $(N_x, N_y, N_z) = (516, 64, 64)$ where (x, y, z) are radial, field-aligned, perpendicular coordinates. The radial resolution corresponds to $0.36\,\mathrm{mm}$. The toroidal domain covers the half torus, so the minimum toroidal number is $n = 2$, equal to the toroidal mode number of the applied RMP. A shifted circular equilibrium is constructed by mimicking the pedestal pressure profile of typical KSTAR H-mode discharges. Pressure and current profiles chosen in this paper are relatively weak compared to actual ones,

in order to focus on the study of the pitch-resonant response. The imposed rotation profile is modeled in a form of $\tanh\left[(\psi_N-1)^2/\Delta\psi_N^2\right]$ with $\Delta\psi_N = 0.2$. The rotation profile is used as the effective rotation in Sec. 3 and Sec. 4 and as toroidal rotation in the calculation of a neoclassical radial electric field in Sec. **??**. The safety factor q increases monotonically from $q_0 = 1.5$ to $q(\psi_N = 1) = 4.1$. The parallel vector potential, $A_\parallel^{\rm vac} = -\psi^{\rm vac}B_0$, corresponding to magnetic perturbations from the system of KSTAR in-vessel coils is calculated in Cartesian coordinates from the Biot-Savart law and transformed into the field-aligned coordinates in the BOUT++ framework.

3 Physics of linear plasma response from two-field model

We consider magnetic plasma responses in a two-field fluid model for a heuristic purpose. Neglecting pressure and parallel velocity fluctuations, the vorticity equation and Ohm's law in a slab geometry can be written in the form of a linear response-drive system. The current gradient (J_0') and the rotation ($V_{e,\perp}$) coupled with RMP drive electrostatic potential and magnetic perturbations in the presence of external vacuum perturbations. Writing in terms of $\psi^{\rm plas}$,

$$L\psi^{\rm plas} = \underbrace{\left(\frac{i}{\gamma}k_\parallel v_A^2 k_\perp^{-2} J_0' + V_{e,\perp}\right)\frac{\delta B_r^{\rm vac}}{B_0}}_{\rm drive}, \tag{2}$$

where $k_\parallel(r = r_0) = 0$ for $m/n = q(r_0)$, $\gamma' = \gamma - ik_y V_{e,\perp}$. The response function L is $L = \left[\gamma' + \eta k_\perp^2 + (k_\parallel v_A^2(k_\parallel k_\perp^2 + k_y J_0'))/\gamma k_\perp^2\right]$. The equilibrium potential in the advection term of the vorticity equation is dropped for simplicity.

Focusing on the drive, RHS of Eq. (2), the presence of $k_\parallel$ in the current-gradient drive is the most significant. The plasma response to J_0' would be kink-mode like in that $\psi_{mn}^{\rm plas}(r_0) \simeq 0$, giving rise to $\delta B_r^{\rm plas} \simeq 0$ and $\delta B_r^{\rm tot} \simeq \delta B_r^{\rm vac}$.

The coupling of $V_{e,\perp}$ to the vacuum field can produce a finite magnetic fluctuation directly at the rational surface through Ohm's law. The response to $V_{e,\perp}$ would be tearing-like, $\psi_{mn}^{\rm plas}(r_0) \neq 0$. When $\gamma = 0$, Eq. (2), locally at the rational surface, reduces to,

$$\delta B_r^{\rm plas} = ik_y\psi^{\rm plas}B_0 = -\frac{1}{1 + i\alpha_{\rm m}^{-1}}\delta B_r^{\rm vac}, \tag{3}$$

where $\alpha_{\rm m} = k_y V_{e,\perp}/\eta k_\perp^2$ is the ratio of a poloidal electron drift rate to a resistive diffusion rate. Zero resistivity in ideal plasmas (i.e., $\eta = 0$) shows a complete screening, $\delta B_r^{\rm plas} = -\delta B_r^{\rm vac}$. One can define a shielding efficiency $\Lambda = |1 - \delta B_r^{\rm tot}/\delta B_r^{\rm vac}|$. Approximately, $\alpha_{\rm m} \sim 1$ gives a 70% shielding of RMPs. The parametrization of the shielding by $\alpha_{\rm m}$ may suggest that the ratio $\alpha_{\rm m}$ could serve as a good physics indicator for resistive effects on pitch resonant responses driven by $V_{e,\perp}$. Then, one may define the critical rotation $V_{e,\perp}^c$ that is necessary for a certain amount of shielding Λ_c, leading to $V_{e,\perp}^c \propto \eta k_\perp^2/k_y$.

The perpendicular length scale $k_\perp^{-1}$ for resistive diffusion is to be determined by considering full dynamics in the radial domain, as done in the context of the layer theory[15]. The perpendicular length scale is dependent on resistivity η. $V_{e,\perp}^c$ may be expressed as $\sim \eta^a$ for a fraction

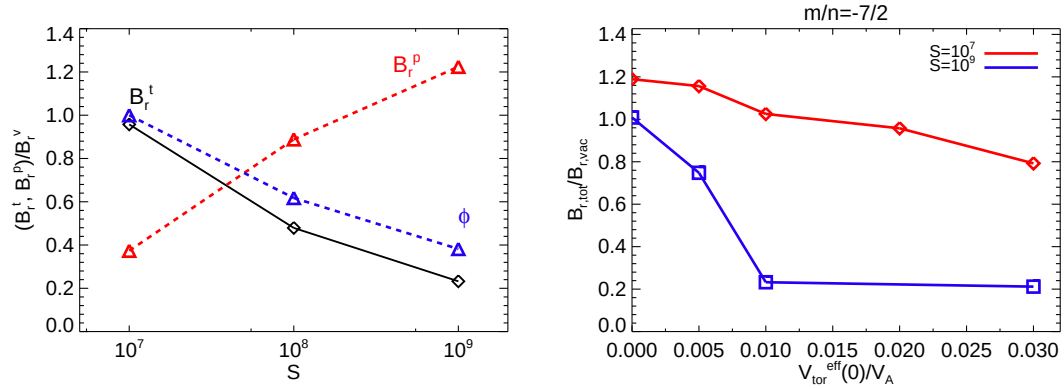

FIG. 1: (a) Dependence of the normalized radial response ($\delta B_r^{plas}/\delta B_r^{vac}$) (red, dot-dashed), magnetic fluctuation $\delta B_r^{tot}/\delta B_r^{vac}$ (black, solid) at $m/n = -7/2$, and the electrostatic potential (ϕ) on Lundquist number S. (b) Dependence of radial magnetic fluctuations $\delta B_r^{tot}/\delta B_r^{vac}$ at $(m, n) = (-7, 2)$ on rotation speed $V_{tor}^{eff}(0)/V_A$.

of RMP shielding. For RMP penetration of a certain fraction Λ_c, the condition $V_{e,\perp} < V_{e,\perp}^c$ may be met qualitatively, where $V_{e,\perp}^c$ is a function of resistivity. The linear relation between the logarithm of rotation and resistivity at fixed shielding is also found in a comprehensive scans of resistivity and plasma rotation for RMP penetration (see Fig. 8(a) in Haskey *et al.* [9]), where the estimated exponent is $a \sim 0.9$.

Although a study of the response function L is necessary for understanding plasma responses, Eq. (2), the distinction between rotation and current-gradient drives is useful in understanding the response, at low resistivity. The features of driving source-dependent plasma responses are clearly demonstrated and confirmed in the numerical simulations.[16]

4 Effects of Resistivity on linear plasma response

In Fig. 1(a), the resistivity effects on plasma responses are shown when $V_{\rm tor}^{\rm eff}(0) = 0.01V_A$. Here the perpendicular flow is represented by the effective toroidal rotation, $V_{\rm tor}^{\rm eff} = B_0 V_{e,\perp}/B_{\rm pol}$ since it provides a sense of how large the flow is. Note that the value $V_{\rm tor}^{\rm eff}(0)$ indicates the core (or pedestal) rotation of the hyperbolic tangent rotation profile, and $V_{\rm tor}^{\rm eff}(r_{-7/2}) \simeq 0.1V_{\rm tor}^{\rm eff}(0)$, where $q(r_{-7/2}) = -7/2$ and $r_{-7/2}/a = 0.96$. As the Lundquist number S increases, $\delta B_r^{\rm plas}$ increases and screens more vacuum field.

The ratio of the total magnetic perturbation to the amplitude of RMP, $\delta B_r^{\rm tot}/\delta B_r^{\rm vac}$, on rotation are shown in Fig. 1(b) for two different values of S. At high resistivity, $S = 10^7$, the rotation $V_{\rm tor}^{\rm eff}(0) \sim 0.01V_A$ allows as strong $\delta B_r^{\rm tot}$ as $\delta B_r^{\rm vac}$ around the rational surface. Even at $V_{\rm tor}^{\rm eff}(0)/V_A \sim 0.03$, the magnitude of a residual magnetic perturbation is relatively large, providing only 20% screening of vacuum perturbations. Note $V_{\rm tor}^{\rm eff}(0) = 0.01V_A \simeq 116\,{\rm km/s}$ and the corresponding $V_{\rm tor}^{\rm eff}(r_{-7/2}) \sim 0.001V_A \simeq 11.6\,{\rm km/s}$ at the rational surface of $m/n = -7/2$. Therefore, the effective rotation corresponding to the critical flow speed $V_{e,\perp}^c$ for $S = 10^7$ is larger than $0.003V_A$. RMP penetration is not critically dependent on $V_{\rm tor}^{\rm eff}$ in this case, due to large $V_{e,\perp}^c$.

At low resistivity, $S = 10^9$, a large fraction of the vacuum field is shielded at $V_{\rm tor}^{\rm eff}(0) \sim 0.01V_A$. In Fig. 1(b), the shielding efficiency Λ increases from 0.2 to 0.8 as $V_{\rm tor}^{\rm eff}(0)/V_A$ increases from 0.005 to 0.01. There is a transitional rotation, i.e., $V_{e,\perp}^c$, for a significant shielding of vacuum perturbation field. This critical rotation at $r = r_{-7/2}$ is $V_{e,\perp}^c B_0/B_{\rm pol} \sim 0.001V_A$ for $S = 10^9$. The square of the perpendicular length scale $k_\perp^{-2}$ scales with $\sim \eta^{0.3}$ at $V_{\rm tor}^{\rm eff}(0) = 0.01V_A$, indicating $V_{e,\perp}^c \sim \eta^{0.7}$. For $S = 10^7$, the critical rotation for 80% shielding would be larger than $0.003V_A \simeq 35\,{\rm km/s}$. Therefore, the good penetration of RMP at high resistivity and the effective shielding at low resistivity can be attributed to large and small $V_{e,\perp}^c$, respectively.

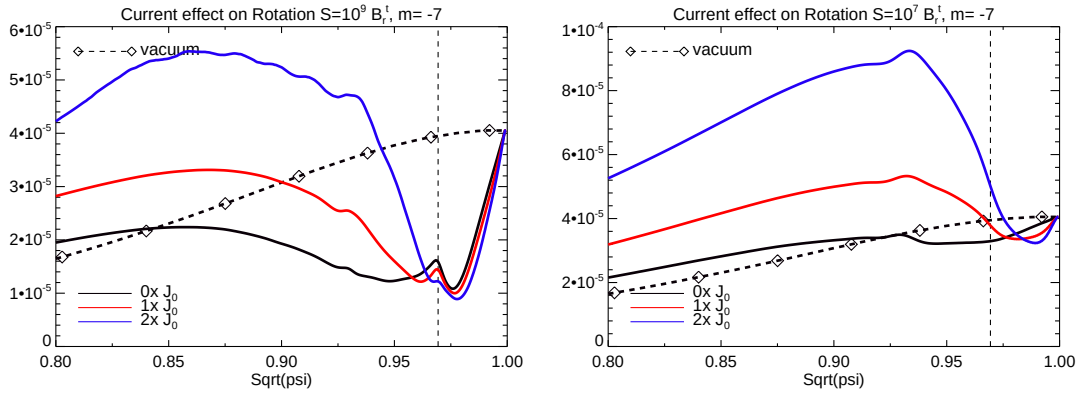

FIG. 2: Radial profiles of the total magnetic fluctuation δB_r^{tot} for $S = 10^9$ (left) and 10^7 (right). Black, red and blue represents the equilibrium current variation $(0, 1, 2) \times J_0$ with vacuum amplitudes (dashed), respectively. The vertical line indicates the rational surface corresponding to $q(r_0) = m_0/n = -7/2$.

Effects of an J_0' on total magnetic fluctuations for high and low Lundquist numbers S are shown in Fig. 2. Again, we investigate $(m_0, n) = (-7, 2)$ in Fig. 2. In ideal cases, as discussed, J_0' does not modify $\delta B_r^{\rm tot}(r = r_0)$ at the resonant rational surface. So the modification is quite weak when $S = 10^9$. In more resistive plasmas, $S = 10^7$, J_0' can significantly enhance the total magnetic field at the rational surface. The enhancement reaches up to 50% by doubling J_0'. This additional enhancement induced by a large current gradient may help RMP penetration at large resistivity. Since this modification is weak at low resistivity, the current-gradient is subsidiary to rotation in terms of RMP penetration at the rational surface.

The current gradient enhances kink responses at $r < r_0$. Since the (m_0, n) perturbation constitutes kink responses for $(m < m_0, n)$ rational surfaces, the corresponding perturbation at $r < r_0$ plays a role of the kink responses at rational surfaces at $r < r_0$. Doubling J_0' can amplify the kink response approximately by a factor of two. In addition, the kink response becomes larger as resistivity increases. This is consistent with the results of a previous computation study[9].

A larger kink response with higher resistivity may need a closer look. In Fig. 2, kink responses can be divided into $\delta B_r^{\rm tot}(r < r_0) = \Delta B_r^{\rm tot}(r) + \delta B_r^{\rm tot}(r_0)$ where $\Delta B_r^{\rm tot}(r) = \delta B_r^{\rm tot}(r) - \delta B_r^{\rm tot}(r_0)$ is a relative enhancement from the perturbation at the resonant rational surface, $r = r_0$. Looking at the maximum, $\rho_{\rm pol} = 0.93$ near the $(m, n) = (-6, 2)$ rational surface, $\Delta B_r^{\rm tot}$ for the case of $2 \times J_0$ is 4.2×10^{-5} when $S = 10^7$ and 3.6×10^{-5} when $S = 10^9$. In

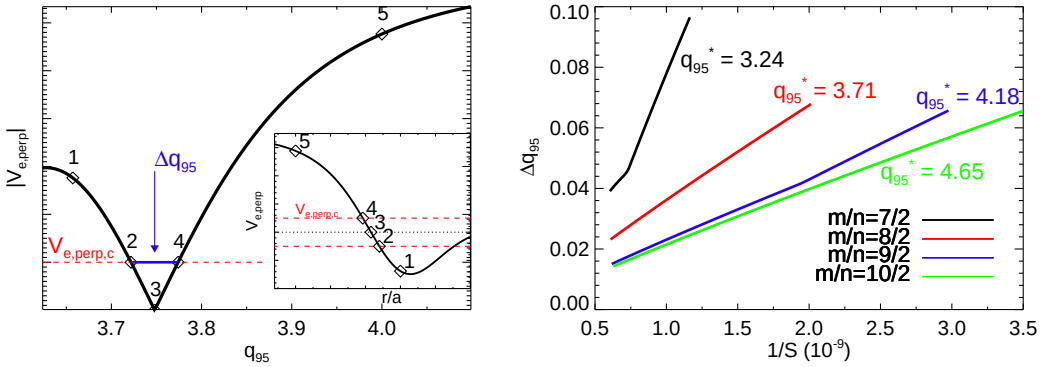

FIG. 3: (a) Schematic diagram of q_{95} window for RMP penetration. (b) The dependence of q_{95} window width for RMP penetration on resonant mode numbers and Lundquist numbers S.

other words, $\Delta B_r^{\rm tot}(r)$ is similar to each other at both Lundquist numbers and the resistive effect on the relative enhancement appears weak. On the while, the base level $\delta B_r^{\rm tot}(r_0)$ does change with resistivity. Its change is affected by the resistive effects on RMP shielding by rotation. Therefore, J_0' determines the relative enhancement $\Delta B_r^{\rm tot}$, while the base level is determined by plasma rotation. This is especially true at low resistivity where J_0' does not modify the magnetic perturbation at $r = r_0$. This suggests that low $V_{e,\perp}$ at the rational surface can be as critical for kink responses as for pitch resonant responses.

A q dependence of RMP penetration due to the low rotation condition at low resistivity can be possibly related to the presence of a q-window for ELM control, which has been observed in some experiments[17]. As a numerical experiment, $V_{e,\perp}$ at rational surfaces are calculated by varying q_{95} with a fixed H-mode like pressure profile, $\sim (1 - \tanh[(r - r_m)/\Delta r])$ where the radial location $r_m = 0.98$ for the maximum gradient and a pedestal width $\Delta r = 0.015$. The safety factor profile, $q = q_0 + (q_{95} - q_0)(r/0.95)^4$ where $q_0 = 1.2$, is varied by changing q_{95}. As q_{95} increases in Fig. 3(a), the rational surface, here corresponding to $m/n = 8/2$, moves inward, in a sequence $1 \rightarrow 2 \rightarrow 3 \rightarrow 4 \rightarrow 5$. The pressure, the pressure gradient and collisionality at the surfaces change accordingly, so does $V_{e,\perp}$ as shown in Fig. 3(a). Qualitatively, the q_{95} window for RMP penetration can be defined as $\Delta q_{95} = q_{95}(4) - q_{95}(2)$ where $q_{95}(2 \text{ or } 4)$ is the value of q_{95} when the rational surface is at position 2 or 4.

Figure 3(b) shows the dependences of Δq_{95} on resistivity $(1/S)$ for various resonant mode numbers. Here, the resonant mode number represents the level of q_{95}. In order for the rational surface with high m/n to be located near $V_{e,\perp} = 0$ position, q_{95} should be high. Each rational surface for m/n =7/2, 8/2, 9/2 and 10/2 passes $V_{e,\perp} = 0$ when q_{95} =3.24, 3.71, 4.18, 4.65. These q_{95} values, denoted by q_{95}^* in Fig. 3(b), can be used as representing values among q_{95}, the values of which are necessary for the RMP penetration. The critical flow is calculated from $V_{e,\perp}^c = c_1 S^{-a}$ with $a = 0.9$ and c_1 satisfying $V_{e,\perp}^c B_0/V_A B_{\rm pol} = 0.001$ for $S = 10^9$. As expected, each $\Delta q_{95}(S)$ indicates that higher resistivity relaxes $V_{e,\perp} = 0$ condition and gives a broader q_{95} window. At low resistivity, Δq_{95} is quite narrow. As q, i.e., q_{95}^* (or resonant m/n), increases, Δq_{95} becomes narrower. Therefore, at lower resistivity and higher q_{95}, the q-window for RMP penetration becomes narrower. This implies that controlling ELMs by RMP needs more fine-

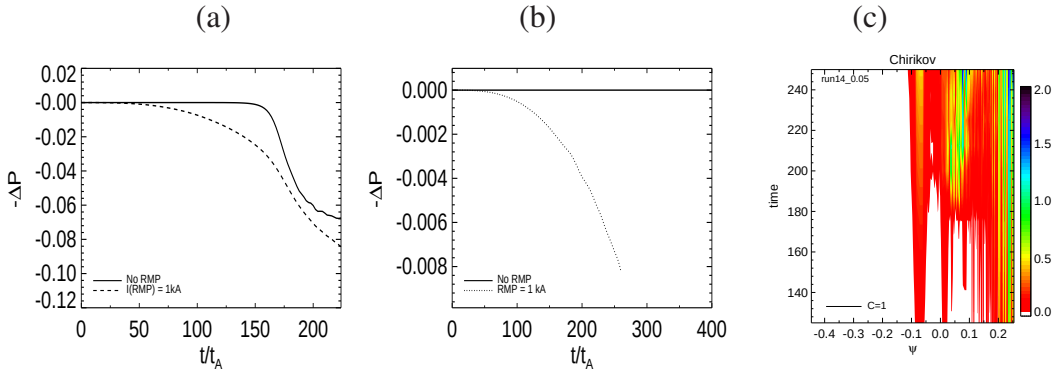

FIG. 4: Changes of pressure with/without RMPs at (a) high and (b) low pressure profiles. Chirikov estimates for the low pressure profile with RMPs.

tuning of plasma conditions and is more challenging. Our results are consistent with recent experiments on ELM control by RMPs[2].

5 Preliminary Results on ELM collapse with RMP

Vacuum magnetic perturbations are applied to the simulations of ELM collapse done in BOUT++ [18]. It is observed that the applied magnetic perturbation induces faster relaxation of $n = 0$ pressure profile in Fig. 4(a), where the ballooning mode is unstable. Also, at the pressure profile where no linear instability and no pressure relaxation are observed without RMP, the application of RMP can induce the relaxation of pressure profiles, as shown in Fig. 4(b) The relaxation is dependent on the amplitudes of the applied RMP.

The observation of larger amplitudes of low-n magnetic fluctuation, $(n > n_{\rm vac})$ such as $m/n = 8/4 = 10/5$ at $q = 2$ surface, may indicate the nonlinear RMP effects on the ELM simulations, where $n_{\rm vac} = 2$ is the toroidal mode number of RMPs. However, the Chirikov parameter in Fig. 4(c) is still below one that is critical for the formation of stochastic field. A responsible mechanism for pressure relaxation is not clear and needs further investigation.

6 Conclusions

In this work, we performed a computational analysis of linear plasma responses to applied RMPs by using a four-field RMHD model[13] implemented in the BOUT++ ++ framework.

From a two-field model, a key physical linear quantity governing the resistivity effect on plasma shielding by rotation turns out to be the ratio between the resistive diffusion rate and the poloidal electron drift rate, $\alpha_{\rm m}$. The small $\alpha_{\rm m}$ can be restated as $V_{e,\perp} < V^c_{e,\perp} \propto \eta^a$ for an RMP penetration condition, where a positive exponent a is expected to be one or less. The condition $V_{e,\perp} < V^c_{e,\perp}(S)$ for RMP penetration combines the zero $V_{e,\perp}$ condition for low-resistivity and an ineffective screening for high-resistivity plasmas into one framework. The low electron rotation condition, $V_{e,\perp} < V^c_{e,\perp}$, is suggested to be also important for the kink response. Kink responses increase with resistivity, as pitch responses do. As a possible implication of the

low flow condition, the q-window for RMP penetration is estimated to be broader with high resistivity and smaller q_{95} at low resistivity. Therefore, the RMP penetration will require a more careful design of plasma parameters at lower resistivity and higher q.

In addition, the preliminary results on the RMP effects on ELM simulations are presented and discussed. RMP may induce pressure relaxation even when the ballooning mode is stable. This needs further investigation.

In conclusion, it is demonstrated that a careful design of plasma experiments is necessary for controlling ELMs for collisionless plasmas and the RMP for ELM control may be effective without complication for resistive plasmas. These observations could be put into one framework by a physical quantity, α_{m}.

7 Acknowledgement

The authors appreciate Dr. B. Dudson and Dr. X. Q. Xu for providing help with BOUT++ and Dr. Gunyoung Park and Dr. Michael Leconte for their constructive comments. This research was supported by the R&D Program through National Fusion Research Institute (NFRI) funded by the Ministry of Science, ICT and Future Planning o f the Republic of Korea (NFRI-EN1541-2), and by the same Ministry under the ITER technology R&D Programme (IN1504-2).

References

[1] H. Zohm, Plasma Phys. Control. Fusion **38**, 105 (1996).
[2] A. Kirk, et al. , Plasma Phys. Control. Fusion **55**, 124003 (2013).
[3] G. T. A. Huijsmans, et al. , Phys. Plasmas **22**, 021805 (2015).
[4] T. Evans, , Nucl. Fusion **48**, 024002 (2008).
[5] C. Paz-Soldan, et al. , Phys. Rev. Lett. **114**, 105001 (2015).
[6] W. Suttrop, et al. , Phys. Rev. Lett. **106**, 225004 (2011).
[7] Y. Liu, A. Kirk, and E. Nardon, Phys. Plasmas **17**, 122502 (2010).
[8] M. Becoulet, et al. , Nucl. Fusion **52**, 054003 (2012).
[9] S. R. Haskey, et al. , Plasma Phys. Control. Fusion **57**, 025015 (2015).
[10] M. F. Heyn, et al. , Nucl. Fusion **48**, 024005 (2008).
[11] E. Nardon, et al. , Nucl. Fusion **50**, 034002 (2010).
[12] N. M. Ferraro, Phys. Plasmas **19**, 056105 (2012).
[13] R. Hazeltine and J. Meiss, Physics Reports **121**, 1 (1985).
[14] B. Dudson, et al. , Computer Physics Communications **180**, 1467 (2009).
[15] F. Waelbroeck, Nuclear Fusion **49**, 104025 (2009).
[16] J. Kim, S. S. Kim, and H. Jhang, Physics of Plasmas **23**, 092502 (2016).
[17] T. Evans, et al. , Nucl. Fusion **45**, 595 (2005).
[18] T. Rhee, et al. , Nucl. Fusion **55**, 032004 (2015).